ACS SyntheticBiology

pubs.acs.org/synthbio Letter

Phenotypic Patterning through Copy Number Adaptation to Environmental Gradients

Published as part of ACS Synthetic Biology virtual special issue "Quantitative Synthetic Biology".

Paige Steppe,*,‖ Camilo Rey-Bedón,‖ Shalni Kumar, Emerald Forrest, Niklas Van Der Wagt, Arnav Tayal, Lev Tsimring, and Jeff Hasty

Cite This: https://doi.org/10.1021/acssynbio.3c00617 Read Online

ACCESS | Metrics & More | Article Recommendations | Supporting Information

ABSTRACT: We recently described a paradigm for engineering bacterial adaptation using plasmids coupled to the same origin of replication. In this study, we use plasmid coupling to generate spatially separated and phenotypically distinct populations in response to heterogeneous environments. Using a custom microfluidic device, we continuously tracked engineered populations along induced gradients, enabling an in-depth analysis of the spatiotemporal dynamics of plasmid coupling. Our observations reveal a pronounced phenotypic separation within 4 h exposure to an opposing gradient of AHL and arabinose. Additionally, by modulating the burden strength balance between coupled plasmids, we demonstrate the inherent limitations and tunability of this system. Intriguingly, phenotypic separation persists for an extended time, hinting at a biophysical spatial retention mechanism reminiscent of natural speciation processes. Complementing our experimental data, mathematical models provide invaluable insights into the underlying mechanisms and guide optimization of plasmid coupling for prospective applications of environmental copy number adaptation engineering across separated domains.

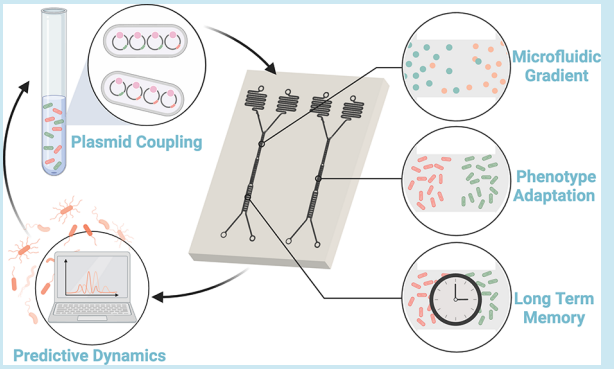

KEYWORDS: *bacterial small ecologies, spatial patterning, plasmid coupling, microfluidics, microscopy*

INTRODUCTION

Having colonized every conceivable niche on Earth, from human tumors to deep-sea vents, microorganisms have evolved diverse strategies to adapt to ever-changing environments. Phenotypic heterogeneity stands out as a pivotal mechanism, allowing genetically identical microbes to exhibit diverse phenotypes and enhance survival across various conditions.[1,2] This adaptability manifests in microbial behaviors such as division of labor in biofilm formation or bet-hedging persistence to endure antibiotic treatments.[1,3−5] From a theoretical standpoint, some molecular heterogeneity is expected. Genetic expression, governed by a limited number of molecules, results in fluctuations in the molecular composition of individual cells within a population.[6,7] While this is intrinsic to any molecular mechanism, microbial genomes have strategically evolved to harness and modulate this molecular stochasticity. This is evidenced in organisms like*Escherichia coli* and *Saccharomyces cerevisiae*, where conserved and essential genes exhibit drastically reduced expression variation compared to metabolic and stress response genes.[8−10] Given the various mechanisms that underlie and regulate phenotypic heterogeneity, such as autoregulation, aging, circadian rhythms, and cell−cell interactions, this versatile strategy is seen not just as a survival tool in nature but also as a promising avenue for crafting robust and adaptive synthetic biological systems.[11]

Recent research has pioneered the concept of plasmid copy number coupling in synthetic multiplasmid systems. Tang and Liu first showed the use of such systems to stably record environmental events by controlling output plasmid ratio.[12] Later works employed dynamic copy number response of coupled plasmids for adaptation to specific environments, in one case directing reinforcement learning within a microbial population and in the other allowing burden reduction of synthetic constructs.[13,14] Specifically, Kumar et al. showed that copy number flexibility in coupled plasmid systems allows populations to minimize encoded metabolic and other cellular burdens as a function of environment.[14] Bacterial cells housing plasmids sustain them at a specific copy number, steered by the autoregulation of the origin of replication. In synthetic biology,

Received: October 4, 2023
Revised: January 25, 2024
Accepted: February 6, 2024

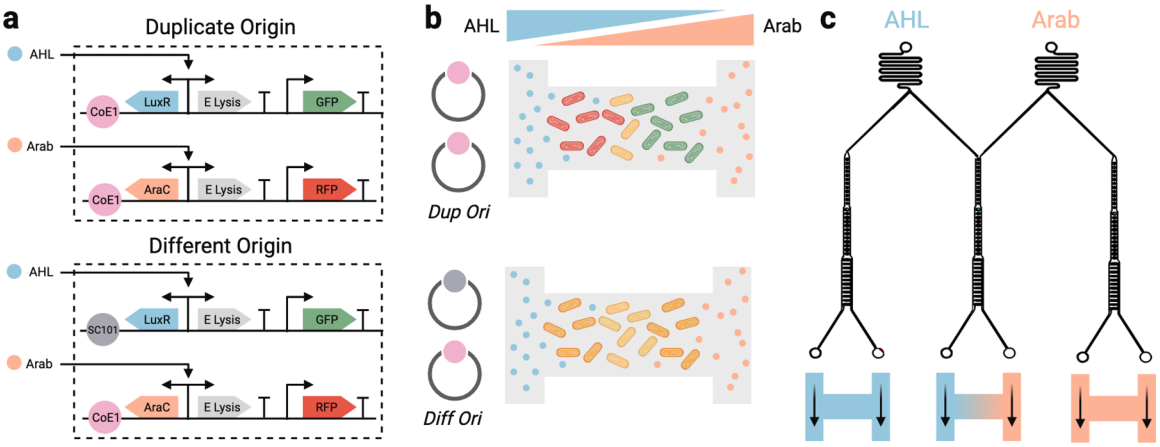

Figure 1. Depiction of the hypothesized spatial distribution of the coupled plasmid system. (a) Overview of dual plasmid genetic circuitry where either AHL or arabinose induces cellular lysis. In the duplicate origin system, both plasmids have the CoE1 origin of replication while in the different origin system the one plasmid has SC101 and the other has CoE1. (b) Representation of expected phenotype distribution across trap of opposing AHL and arabinose gradients. (c) Layout of the microfluidic device with continuous cell cultivation chambers of 50, 100, and 200 μm in either inducer or a gradient of the two.

orthogonal origins of replication are typically employed when integrating multiple plasmids into a cell, a necessary approach for stable maintenance of the copy number for each construct. However, when identical origins of replication are used across different constructs, it was observed that engineered bacterial populations could dynamically adjust each plasmid's copy number in response to environmental condition. This deliberate induction of heterogeneity in the copy number of independent constructs sets the stage for bet-hedging during environmental fluxes, where certain copy number ratios become advantageous. Termed "plasmid coupling", this mechanism enables bacterial populations to leverage phenotypic heterogeneity in ways that echo the natural tactics employed by microbes in variable environments.[15]

To date, much synthetic biology research operates under the assumption of "well-mixed" conditions. To prepare engineered populations for dynamic interaction with complex, non-homogeneous environments there is a need for both quantitative measurement and model-driven optimization of phenotypically variable populations in a multidimensional context. In this study, we build a framework for simulation and testing of the spatiotemporal dynamics of plasmid coupled strains within controlled 2D environments. Using cutting-edge microfluidic technology, we can continuously monitor bacterial proliferation across an adjustable gradient of inducers. Complementing our experimental investigations, we developed a stochastic computational model that simulates the hypothesized spatial separation of phenotypes, providing a theoretical framework that supports our empirical observations and offers predictive insights. Our combined experimental and computational results reveal pronounced phenotypic divisions in bacterial populations when exposed to environmental inducer gradients, underscoring plasmid coupling's potential as an adaptive tool for higher order complexity. Beyond this, our work paves the path toward deployment of differentiating strains in practical scenarios, such as selective drug delivery, dynamic bioproduction, and communication between niche-specific subpopulations. This approach allows for environmental genetic modulation, bypassing the need for sense and response circuits and thereby emulating nature's phenotypic plasticity.

RESULTS AND DISCUSSION

Microfluidic Device for Plasmid Copy Number Control.

Previous work on plasmid copy number regulation has successfully created small-molecule inducible copy number and mutated copy number variants.[16,17] Recently, single strains carrying coupled plasmid systems have been developed which are capable of copy number-mediated differentiation and thereby population adaptation.[14,18] The single strain contains two distinct plasmids with shared replication machinery, coupling their copy numbers and generating a new source of heterogeneity. The above work with colE1 plasmids has shown that due to shared replication inhibition, two distinct colE1 constructs will share a total copy number but have a flexible distribution of each plasmid. Plasmid copy number can be visualized by a constitutively expressed unique fluorescent marker per construct, where the fluorescence ratio represents the overall plasmid distribution. Here, we employed strains containing negative environmental burden in the form of induced production of protein phi X-174 (E-Lysis) which disrupts membrane integrity leading to a halt in ATP production and eventually lysis in Gram-negative bacteria[19,20] (Figure 1a). Each plasmid in the coupled system has a unique environmental lysis inducer, either *N*-acylated-L-homoserine lactones (AHL) or arabinose, plus a unique reporter, either GFP or RFP, respectively. This coupled plasmid system with negative environmental feedback was kindly donated from Kumar et al.[14] and served as a model system for testing bacterial self-adaptation to environmental conditions across spatial gradients. Figure 1b demonstrates the hypothesized spatial phenotypic plasticity with a coupled plasmid system compared to uniform expression expected from traditional compatible plasmids.

We developed a multidimensional microfluidic device capable of producing and maintaining superimposed continuous gradients of small molecules across a bacterial cultivation chamber. This is achieved by connecting two flowing channels, each carrying a small molecule, with a bacterial trap of 1 μm in height for 2-D microscopy of a monolayer of cells. This device allows us to superimpose opposing gradients of AHL and arabinose to enable spatial patterning of the environmentally responsive coupled plasmid strain (Figure 1b). When both inlet sources have equal flow rates, a continuous steady-state gradient

https://doi.org/10.1021/acssynbio.3c00617
ACS Synth. Biol. XXXX, XXX, XXX−XXX

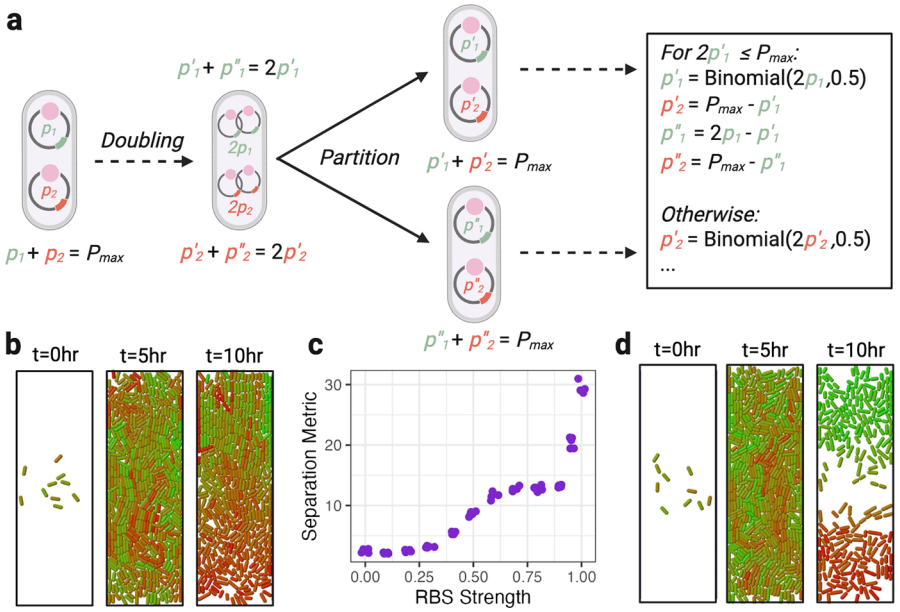

Figure 2. Computational model for spatial distribution of plasmid coupling. (a) Schematic diagram of binomial plasmid partitioning during cell division, restricted to a total copy number of p_{max}. (b) Snapshots of cell chamber during simulation of weak arabinose RBS relative to AHL RBS. (c) Effect of arabinose RBS strength on final trap separation ($n = 5$). (d) Snapshots of cell chamber during simulation of balanced arabinose and AHL RBS strengths.

of environmental inducers is generated across the cell chamber. The device also carries multiple of three types of trap lengths of 50, 100, or 250 μm to probe different gradient spans based on the inducer's diffusivity.[21] Upholding this basic design principle, two distinct chip variations were constructed. In the first design, each inlet channel immediately flanks either side and fully feeds an entire trap. This creates three unique cell cultivation chamber conditions from the same inlet media sources of only media 1, only media 2, and gradient from media 1 to media 2 (Figure 1c). The second design has two fully independent gradient-generating microfluidic systems within a single chip allowing for two device technical replicates per experiment (Figure S1b). To further optimize our experimental setup and anticipate potential outcomes, it is vital to generate a computational framework that can predict the behavior of bacterial populations in our proposed coupled plasmid system.

Modeling of Copy-Number Based Patterning. To model the spatiotemporal dynamics of bacterial colonies in our microfluidic devices, we used an agent-based approach. There have been a number of mechanistic agent-based models of cellular populations described in the literature that share the same general methodology.[22−26] Briefly, individual cells are represented as spherocylinders that increase in length based on their growth rate and divide once reaching a set length. Cells repel contact with each other and the chamber walls. Each cell also carries two variables representing the number of plasmids of types 1 and 2. These plasmid numbers are updated on cell division by doubling prior to binomial partitioning between the two daughter cells, as depicted in Figure 2a. Thus, daughter cells retain memory of the plasmid distribution of the mother cell; however, gradually this memory is lost, and the distribution returns to the equilibrium. (See Methods for further details).

To model the experiments with plasmid separation by external signals, we allowed the cell colony in our simulations to grow for 5 h to fill up the chamber, after which we applied two different chemical inducers (AHL and arabinose) on two opposing sides of the chamber. We assumed that the concentration of each inducer decays inward exponentially, according to the distributions

$$\mathrm{AHL}(y) = \mathrm{AHL}_0 \exp[\alpha(y - L_y/2)] \quad (1)$$

$$\mathrm{Ara}(y) = \mathrm{Ara}_0 \exp[-\alpha(y + L_y/2)] \quad (2)$$

Since experimentally each inducer activates a lysis gene on the plasmid that carries the corresponding promoter, the probability of a cell lysing depends on both the local concentration of the inducer and the number of its cognate plasmids. We remove a cell i from the colony if either of the two conditions is fulfilled: $\mathrm{AHL}(y^i)p_1^i > \epsilon$ or $\mathrm{Ara}(y^i)p_2^i > \epsilon$. Here y_i is the location of cell i, $p_{1,2}^i$ are the copy number of plasmids of both types in that cell, and ϵ is a nominal threshold value. Sample snapshots of a typical simulation illustrate a quick separation of "red" and "green" cells inside the computational domain (Figure 2d). The distributions of p_1 and p_2 quickly become bimodal, and the average numbers of plasmids in the top and bottom halves of the computation domain strongly diverge (Figure S7a,b). We further simulate the dynamics of a population under the spatially uniform presence of both inducers (Figure S9). In this case, increased lysis pressure selects for cells with intermediate plasmid ratios and thereby stabilizes the population copy number.

To probe the robustness of our model, we explored the effect of an imbalance in the inducer sensitivity between the plasmids. Experimentally, this would correspond to mutating (and weakening) the RBS sequence at one of the plasmid's lysis gene promoters. In our computer simulation, we modified the second condition for the cell lysis by $\mathrm{RBS}{\cdot}\mathrm{Ara}(y^i)p_2^i > \epsilon$ with the parameter RBS < 1. For a weak RBS = 0.1, red-shifted cells are less prone to lysis and dominate throughout the chamber, however, this domination gradually weakens away from the lower open side (Figure 2b). Unlike the case of balanced lysis, the average copy numbers of plasmids in the top and bottom halves show much weaker separation. We quantified this

https://doi.org/10.1021/acssynbio.3c00617
ACS Synth. Biol. XXXX, XXX, XXX−XXX

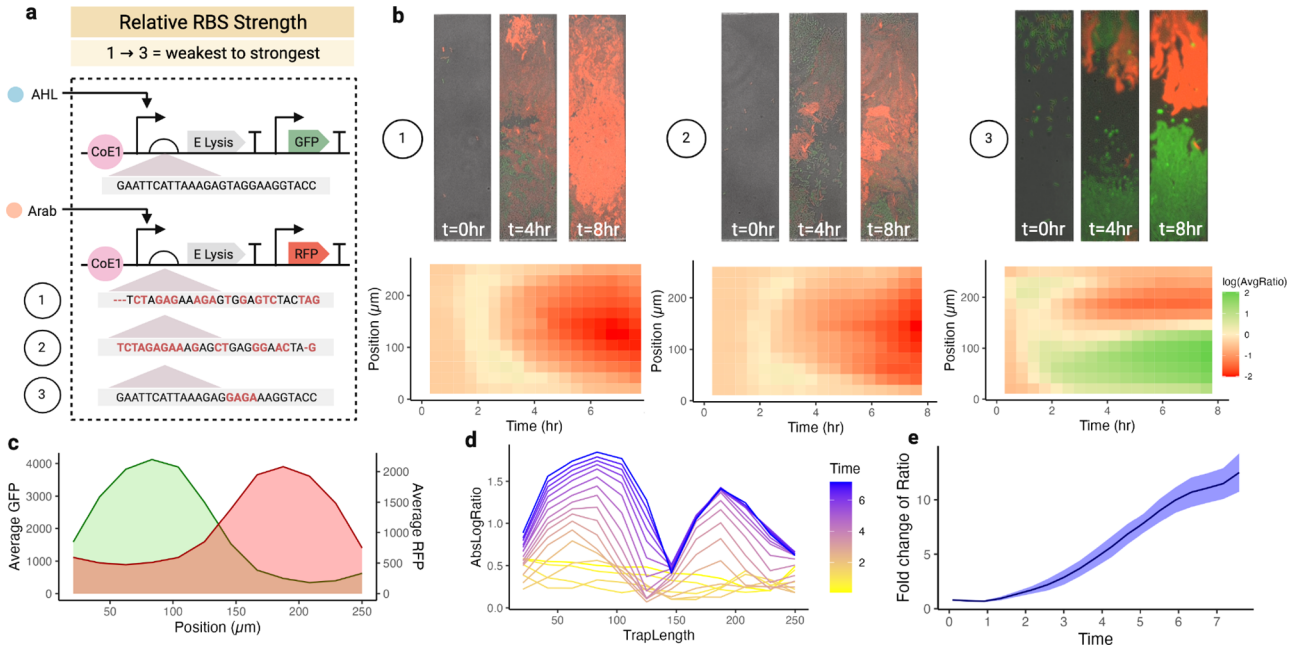

Figure 3. Copy number based phenotype separation. (a) Sequencing of mutations generated in RBS library and relative strength. (b) Snapshots from microfluidic runs on RBS library showcasing observed phenotype separation and heat maps summarizing fluorescent localization over time. (n = 12). (c) Average GFP and RFP fluorescence across a single trap at 4 h (n = 12). (d) Ratio of fluorescent proteins across trap length over time. (e) Separation metric across all 12 traps over 8 h.

separation by the separation parameter S which was computed as follows:

$$S = \frac{\langle \langle p_2 \rangle_t / \langle p_1 \rangle_t \rangle_t}{\langle \langle p_2 \rangle_b / \langle p_1 \rangle_b \rangle_t}$$

where as before $\langle p_{1,2} \rangle_{t,b}$ are the average copy numbers of plasmids $p_{1,2}$ in top and bottom halves, respectively, and the outside brackets indicate averaging over time after the steady state has been reached. Figure 2c shows a rather nontrivial behavior of this separation parameter as we varied the RBS parameter. For small RBS, when one plasmid dominates, this parameter is small (close to 2 in our simulations). It then grows gradually with RBS and reaches a plateau of about S = 15 between RBS = 0.6−0.9, and then it grows rapidly at very large RBS and eventually it reaches a large value 30 for RBS = 1. Our computational modeling provides insights into the anticipated spatiotemporal patterns in our experimental setup, emphasizing the complex interplay between induction strength and population-level behavior.

Phenotype Patterning from Environmental Fluctuations. Our preliminary spatial modeling of the coupled plasmid system underscored the importance of balancing RBS strength across both plasmids to achieve phenotypic separation. Therefore, we investigated three unique coupled plasmid *E. coli* MG1655 strains with variable RBS sequences upstream of arabinose-inducible lysis (Figure 3a). After a lysis screening of RBS mutants, we selected strains here named strains 1, 2, and 3, representing weak, medium, and strong RBS lysis. Using microfluidics, as described in methods, exponential phase cells were loaded at low density into cell chambers and exposed to superimposed opposing gradients from 200 nM AHL and 0.02% arabinose. Then the cells were able to colonize and adapt to this heterogeneous environment while being monitored through fluorescent microscopy. For Strain 1, during the first 3 h of growth, cells appeared to follow their initial seeding pattern, highlighted by the mixed populations of RFP-shifted and GFP-shifted cells representing high arabinose-induced plasmid and high AHL-induced plasmid copy number, respectively (Figure 3b). However, starting at 4 h and continuing for the remainder of the experiment, the entire cell trap was taken over by high RFP expressing cells indicating a preference for high arabinose plasmid copy number independent of the gradient (Figure 3b). This indicates that the weak lysis induction allows RFP-shifted cells to thrive even at the highest arabinose concentration. Due to this advantage in fitness, they quickly overgrow and displace GFP-shifted cells from the initial mixed heterogeneous population.

Strain 2 behaved similarly to Strain 1 with an initially mixed population for the first 3 h followed by the majority of cells having high arabinose-induced copy number ratio and low AHL-induced copy number ratio. Despite both strains preferring high arabinose-induced copy number, Strain 2's magnitude of red fluorescence is lower than Strain 1 indicating improvement toward balanced plasmid coupling (Figure 3b). For Strain 3, a notable separation between plasmid copy preference was achieved within the 250 μm cell chambers, indicated by clear differential localization of green and red fluorescence to opposing trap ends after 4 h and becoming starker thereafter (Figure 3c,d,e). In chamber sizes of 50 μm and 100 μm, the higher inducer pressure led Strain 3 to follow initial seeding patterns as opposed to environmental selection suggesting a spatial limit in phenotypic separation that might be expanded with fine-tuning of inducer gradient (Figure S3). Interestingly, as the cells populated the trap, we observed an illusion of population swarming along the trap, likely due to balanced growth and death rates at the beginning of each experiment. In addition, a boundary layer lacking cell growth emerged in the middle of the cell trap completely dividing the two subpopulations of RFP-shifted and GFP-shifted cells (Movie

https://doi.org/10.1021/acssynbio.3c00617
ACS Synth. Biol. XXXX, XXX, XXX−XXX

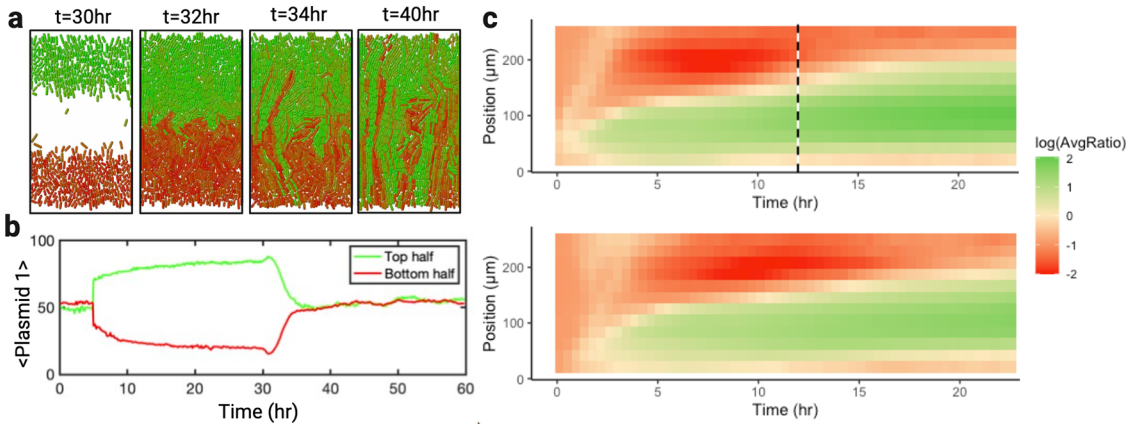

Figure 4. Copy number based memory postinduction. (a) Simulation results highlighting the expected relaxation after media swapping. (b) Quantification of Plasmid 1 copy number in the top and bottom half of the simulation trap. (c) Fluorescent quantification across microfluidic run where the dashed line indicated removal of inducers from media (n = 12).

S1). This behavior, observed over a prolonged period, highlights the influence of environmental gradients on phenotypic outcomes among genetically identical cells thanks to plasmid copy number heterogeneity. In addition to lysis as the main driving force for preferential plasmid separation, secondary effects of specific circuit induction could lead to a reduced growth rate or plasmid replication of cells carrying larger numbers of induced plasmids. This added feedback could enhance spatial separation in nontrivial ways and also may operate at slower time scales.[27] Strikingly, this separation mimics the effects of phenotypic plasticity, where drastic phenotypic differences can emerge from the same genetic background based on external cues.

For controls, Strain 3 was also run in our microfluidic device containing cell cultivation chambers with a single uniform inducer presence. Strain 3 followed the expected patterning with dominant arabinose-induced copy number ratio in only 200 nM AHL conditions and dominant AHL-induced copy number ratio in only 0.02% arabinose conditions (Figure S3, Movies S2 and S3). These results align with the findings of Kumar et al. and highlight that selective pressure from a single homogeneous inducer causes rapid lysis of subpopulations carrying high copy number of the induced plasmid and thereby leads to decline of this plasmid in the overall population.[14] A fourth strain with different origins of replication on each plasmid served as a comparison to traditional compatible plasmids. Without plasmid coupling the microfluidic experiments showed Strain 4 was unable to adapt to the environmental cues and large-scale cell death occurred across all cell traps (Figure S4).

Long-Term Genetic Memory of Population Phenotype. To further probe the longevity of plasmid-mediated phenotypic segregation, additional microfluidic experiments with inducer removal were conducted on Strain 3. As anticipated from our prior experiments, all cell traps showed complete phenotype separation in 4 h. After 12 h, all inducers were removed from half of the cell traps, releasing inducer-mediated environmental pressure. Thereafter, the population still maintained a clear separation for several hours until GFP-shifted cells began to slowly take over the cultivation chamber (Figure 4c, Movie S4). Interestingly, this was also the case for traps with sustained long-term inducer cues. This slow trend toward GFP-shifted dominance sheds light on the intricacies of plasmid-mediated phenotypic dynamics. While the external inducers play a crucial role in driving phenotypic differentiation in the initial stages, notably within the first 4−8 h, the system seems to transition toward a new equilibrium favoring the green phenotype independent of these cues. A plausible explanation for this shift might lie in the evolutionary and cellular mechanics that are at play. If the AHL-induced plasmid imparts a slightly reduced burden on the cellular machinery than does the arabinose-induced counterpart, cells harboring this GFP-expressing plasmid could exhibit a fitness advantage over time. Additionally, following inducer removal, leaky expression from the pBAD promoter or biases in plasmid replication could result in the apparent dominance of GFP-shifted cells. Such marginal benefits can result in a significant alteration in the phenotypic landscape of the bacterial population. Concurrently, sporadic mutations that impact lysis induction differently could also accelerate this green-dominant trend. This result illustrates the population's adaptive strategy to optimize growth and sustainability, despite the constraints of earlier external pressures.

To supplement these findings, we used our computational model to simulate relaxation from a plasmid-separated regime after inducer removal. Similar to experimental runs, the simulations showed the maintenance of phenotypic separation for the first few hours after the removal of inducers. However, unlike our observations in microfluidics, the simulated population returned to a mixed heterogeneous state soon after. Based on our model, we hypothesized that this memory effect should be more pronounced for high copy number p_{max} since a larger pool of plasmids reduces stochastic effects and slows down the stochastic copy-number drift (Figure S8). Surprisingly, we did not observe a strong memory effect for all values of copy numbers tested, presumably because the red-shifted and green-shifted cells on the edges of the chamber get quickly pushed away by growing cells in the middle of the chamber that have approximately equal values of p_1 and p_2. Moreover, there was not a slow takeover of green-shifted cells in the simulations as seen experimentally with GFP-shifted cells, presumably due to the precisely equal plasmid burden in the model and a lack of other natural factors, such as spontaneous mutations or physical interactions between biofilms and inducer removal rates present in the complexity of the microfluidic experiments. While the computational model offers insightful predictions, the discrepancies observed with experimental results highlight the intricate complexities of biological systems. Our findings emphasize the essential interplay between genetic

https://doi.org/10.1021/acssynbio.3c00617
ACS Synth. Biol. XXXX, XXX, XXX−XXX

factors, molecular stochasticity, and environmental influences, underscoring the need for a synergistic approach between modeling and empirical studies in understanding microbial adaptability and its engineering for synthetic applications.

CONCLUSIONS

Generating spatial patterns in engineered communities has been of great interest to synthetic biologists hoping to gain insight into the morphogenesis of natural systems.[28] To date, gene-regulatory networks carrying incoherent feedforward loops have been a classical method for generating phenotypic patterns in response to simple environmental gradients.[29,30] Here we show how the use of plasmid coupling for the generation of population phenotypic diversity enables an initially clonal population to respond to nonhomogenous external conditions. Unlike traditional sense-and-respond circuitry, we demonstrate the use of cellular burden as a driving force for spatial differentiation by introducing copy number heterogeneity. Visualization of population spatial dynamics within a continuous microfluidic device serves as a tractable model system for studying the externally controlled spatial organization. In addition, fitness-based population response allows for dynamic adaptation to fluctuating conditions on time scales distinct from transcriptional circuits. For example, phenotypic diversity allows immediate survival of subpopulations in the face of extreme lytic pressure, while plasmid inheritance creates long-term memory of spatial distribution in the absence of selection. Many of these features reflect those of natural systems that are robust to varying environments.

By employing plasmid coupling as an alternative to traditional gene-regulatory networks, we demonstrate a unique approach for a clonal population to respond to various external conditions. Using cellular burden for spatial differentiation, this system can house multiple constructs with specific genetic circuits, where the cells can adapt and activate the most appropriate pathway based on their immediate environment. This research provides a proof of concept for leveraging this recently developed technology for synthetic biology applications. For instance, in the realm of environmental sensing and remediation, bacteria equipped with multiple circuits could become dynamic responders by degrading pollutants specific to a given environment. In a medical context, the same principle could lead to targeted drug delivery, with bacteria activating therapeutic circuits in correspondence with tumor microenvironment gradients, increasing conditional delivery resolution. Moreover, in industrial microbiology, the adaptability of production organisms could be harnessed to optimize the synthesis of valuable compounds based on available feedstocks or environmental parameters. Therefore, the capabilities demonstrated in this work through plasmid coupling technology in spatial patterning emphasize its potential for application in diverse fields, from environmental sensing to targeted therapeutics.

METHODS

Microfluidics and Microscopy. The microfluidics techniques are similar to those described previously by our group.[31] Our microfluidic devices were constructed from PDMS (polydimethylsiloxane), which was molded and baked on a silicon wafer with micrometer-scale features formed by cross-linked photoresist. After about 12 h of baking at 65 °C, the PDMS was peeled from the wafer and features were transferred onto the PDMS. Individual devices were then cut out of the baked PDMS and holes were punctured in the devices to allow for the connection of fluid lines. The devices were then bonded onto coverslips and placed on a microscope stage for cell loading and imaging. Before each experiment, the devices were left for 45 min in a vacuum chamber. After taking the device out of the vacuum chamber, 10 μL droplets of cells were positioned on the outlets. Similarly, 10 μL droplets of sterile media were placed on the inlet openings. The media used contained LB and antibiotics of appropriate concentration along with either 200 nM AHL or 0.02% arabinose sugar. In every case, 0.075% Tween20 was added to the medium to prevent cells from sticking to the PDMS walls. After all the chip features were wetted, fluid lines were connected to the devices from various syringes supplying media or acting as waste reservoirs. The flow direction in the device was controlled by changing the relative heights between the relevant syringes, resulting in hydrostatic pressure driven flow. Images were acquired using a Nikon Ti-2 microscope. The microscope was housed in a plexiglass incubation chamber maintained at 37 °C by a heating unit. Phase-contrast images were taken at 20× magnification. For mCherry the fluorescence exposure time was 50 ms at 50% intensity, while for GFP the fluorescence exposure time was 40 ms at 50% intensity. Images were taken every 10 min for each experiment.

Description of Agent-Based Model. In our simulations we used the agent-based code developed in ref 26 (the details of the computational algorithm and its implementation can be found in the Supporting Information to that paper), and adapted it for our purposes. Each individual bacterial cell is modeled as an elongating and dividing spherocylinder. The cell increases its length exponentially with a nominal growth rate $\gamma = 1.36\ \mathrm{h}^{-1}$ that corresponds to cell doubling time 0.5 h. When the cell length reaches a certain predetermined value l_{max}, the cell divides into two collinear daughter cells of lengths $l_{max}/2$ touching by their newly formed poles. The cells in our case are nonmotile, so they only move when they experience external forces, typically from neighboring cells. Whenever two cells overlap, they experience repulsion forces at the point of contact that scale with the overlapping distance d according to (typically) a Hertzian law $F \sim d^{3/2}$. They also experience repulsive forces from solid walls (that are computed similarly) and friction forces from the bottom or top of the chamber and the surrounding fluid. Since cells are very small and move slowly, a typical Reynolds number for cellular motion is very small, and the Newton law describing cell motion can be simplified to ignore inertia effects. Thus, the cell velocity is simply proportional to the vector sum of all forces, and the cell angular velocity is proportional to the sum of all momenta.

For our simulations, we confined all spherocylinders to a monolayer in the x, y plane to reflect the design of our microfluidic chambers. The cells were grown in a rectangular domain of width L_x and length L_y. As in experiment, the walls at $x = \pm L_x/2$ were solid, and the walls at $y = \pm L_y/2$ were open, so as soon as the center of mass of a cell crosses those virtual walls, the cell is immediately removed from the colony. Second, we endowed all cells with two internal variables, p_1 and p_2 for the copy numbers of plasmids of type 1 and 2, respectively. We assume that the total number of both plasmids in every cell is fixed, $p_1 + p_2 = p_{max}$. Furthermore, we assume that the plasmid copy numbers do not change during the life cycle of individual cells. However, at cell division, daughter cells get random numbers of plasmids 1 and 2 in approximate proportion to their fraction in the mother cells that add up to p_{max}. We perform this partition by splitting the cell division event into two substeps: in

https://doi.org/10.1021/acssynbio.3c00617
ACS Synth. Biol. XXXX, XXX, XXX−XXX

the first the number of plasmids in the cells doubles to $2p_1 + 2p_2 = 2p_{max}$, and then each plasmid is placed randomly into one of the two daughter cells (see Figure 2a for details).

When initializing a run with a small seed population, each cell has a random copy number p_1 of plasmids of type 1 drawn from a binomial distribution Bin(p_{max}, 0.5), and the number of plasmids of type 2 is $p_2 = p_{max} - p_1$.

Molecular Cloning and Cell Culture. All plasmids were transformed into the *E. coli* strain MG1655. Strains were cultured in lysogeny broth (LB) with 20 μg mL^{-1} chloramphenicol and 60 μg mL^{-1} spectinomycin in a 37 °C shaker. Primer sequencing was conducted on all plasmids within the study. Sequencing identified the arabinose RBS mutations and the AHL RBS described in (Figure 2a). For microfluidic experiments, the appropriate *E. coli* strains were seeded from a −80 °C glycerol stock into 1 mL of LB with appropriate concentrations added and incubated at 37 °C. Samples were monitored for an OD of 0.1 every 20 min and measured at OD600 using a DU 740 Life Science UV−vis spectrophotometer.

Data Analysis. Fluorescence intensity profiles were obtained by analyzing frames from the fluorescent channel recorded on a Nikon Ti-2. The mean fluorescence intensity was calculated by first identifying the trap bounds and parsing them into 12 equiv subsections. The mean value of both the RFP and GFP fluorescent channels were calculated with np.mean() for each subsection and normalized with a trap image prior to loaded cells. Log of the GFP/RFP ratio was plotted following normalization for visualization within heatmaps and calculation of the *S*, separation metric, defined previously.

■ ASSOCIATED CONTENT

Supporting Information

The Supporting Information is available free of charge at https://pubs.acs.org/doi/10.1021/acssynbio.3c00617.

Details on microfluidic chip design and fabrication, additional simulation results with no inducer or both inducers without spatial gradients, and the results of all microfluidic chip runs including single inducer controls (PDF)

Movie S1: Strain 3 in microfluidic device separating under dual inducer gradient (AVI)

Movie S2: Strain 3 in microfluidic device under 0.02% Arabinose induction (AVI)

Movie S3: Strain 3 in microfluidic device under 200 nM AHL induction (AVI)

Movie S4: Strain 3 in microfluidic device under 12 hours of dual inducer gradient followed by 12 hours of no induction (AVI)

Plasmid sequences (ZIP)

■ AUTHOR INFORMATION

Corresponding Author

Paige Steppe − *Department of Bioengineering, University of California San Diego, La Jolla, California 92093, United States;* orcid.org/0000-0002-3447-9393; Email: psteppe@ucsd.edu

Authors

Camilo Rey-Bedón − *Molecular Biology Section, Division of Biological Sciences, University of California San Diego, La Jolla, California 92093, United States*

Shalni Kumar − *Department of Bioengineering, University of California San Diego, La Jolla, California 92093, United States*

Emerald Forrest − *Synthetic Biology Institute, University of California San Diego, La Jolla, California 92093, United States*

Niklas Van Der Wagt − *Synthetic Biology Institute, University of California San Diego, La Jolla, California 92093, United States*

Arnav Tayal − *Department of Bioengineering, University of California San Diego, La Jolla, California 92093, United States*

Lev Tsimring − *Synthetic Biology Institute, University of California San Diego, La Jolla, California 92093, United States;* orcid.org/0000-0003-0709-3548

Jeff Hasty − *Department of Bioengineering, University of California San Diego, La Jolla, California 92093, United States; Molecular Biology Section, Division of Biological Sciences and Synthetic Biology Institute, University of California San Diego, La Jolla, California 92093, United States*

Complete contact information is available at: https://pubs.acs.org/10.1021/acssynbio.3c00617

Author Contributions

[‖]P.S. and C.R.B. contributed equally to this work. All empirical experiments were performed by P.S., C.R.B., S.K., E.F., and A.T.; Computational model and simulations were developed by N.V. and L.T.; Data analysis and experimental design were performed by P.S., C.R.B., S.K., E.F., and A.T.; This article was drafted by P.S., C.R.B., S.K., and L.T., with contributions of revision by E.F., A.T., N.V, L.T., and J.H.; All the authors read and approved the final manuscript.

Notes

The authors declare the following competing financial interest(s): J.H. declares that he is a co-founder of GenCirq Inc, which focuses on cancer therapeutics. He is on the Board of Directors and has equity in GenCirq. His spouse is employed part time by GenCirq for bookkeeping and employee support with Human Resources.

■ ACKNOWLEDGMENTS

This work was supported by the National Institute of Biomedical Imaging and Bioengineering (Grant No. R01 EB030134). Paige Steppe was supported in part by the National Science Foundation Graduate Research Fellowship Program (NSF GRFP) under Grant No. (DGE-2038238). Shalni Kumar was supported in part by the NSF GRFP under Grant No. (DGE-2038238). Shalni Kumar was also supported by the NIH-sponsored Quantitative Integrative Biology Training Grant (No. 5T32GM127235). The authors thank Andrew Lezia for donation of Strains 1, 2, and 3 used in this study. All figures were created using BioRender.com. TOC Graphic is adapted from "Microfluidic Device for Electronic Discrimination of T cells by Activation State", by BioRender.com (2023). Retrieved from https://app.biorender.com/biorender-templates.

■ REFERENCES

(1) Ackermann, M. A functional perspective on phenotypic heterogeneity in microorganisms. *Nat. Rev. Microbiol.* **2015**, *13*, 497−508.

(2) Del Vecchio, D.; Qian, Y.; Murray, R. M.; Sontag, E. D. Future systems and control research in synthetic biology. *Annual Reviews in Control* **2018**, *45*, 5−17.
(3) Reyes Ruiz, L. M.; Williams, C. L.; Tamayo, R. Enhancing bacterial survival through phenotypic heterogeneity. *PLOS Pathogens* **2020**, *16*, No. e1008439.
(4) Grimbergen, A. J.; Siebring, J.; Solopova, A.; Kuipers, O. P. Microbial bet-hedging: the power of being different. *Curr. Opin. Microbiol.* **2015**, *25*, 67−72.
(5) Armbruster, C. R.; Lee, C. K.; Parker-Gilham, J.; De Anda, J.; Xia, A.; Zhao, K.; Murakami, K.; Tseng, B. S.; Hoffman, L. R.; Jin, F.; Harwood, C. S.; Wong, G. C.; Parsek, M. R. Heterogeneity in surface sensing suggests a division of labor in Pseudomonas aeruginosa populations. *eLife* **2019**, *8*, No. e45084.
(6) Raj, A.; Van Oudenaarden, A. Nature, Nurture, or Chance: Stochastic Gene Expression and Its Consequences. *Cell* **2008**, *135*, 216−226.
(7) McAdams, H.; Arkin, A. Stochastic mechanisms in gene expression. *Proc. Natl. Acad. Sci. U. S. A.* **1997**, *94*, 814−819.
(8) Newman, J. R. S.; Ghaemmaghami, S.; Ihmels, J.; Breslow, D. K.; Noble, M.; DeRisi, J. L.; Weissman, J. S. Single-cell proteomic analysis of S. cerevisiae reveals the architecture of biological noise. *Nature* **2006**, *441*, 840−846.
(9) Bar-Even, A.; Paulsson, J.; Maheshri, N.; Carmi, M.; O'Shea, E.; Pilpel, Y.; Barkai, N. Noise in protein expression scales with natural protein abundance. *Nat. Genet.* **2006**, *38*, 636−643.
(10) Silander, O. K.; Nikolic, N.; Zaslaver, A.; Bren, A.; Kikoin, I.; Alon, U.; Ackermann, M. A Genome-Wide Analysis of Promoter-Mediated Phenotypic Noise in Escherichia coli. *PLoS Genetics* **2012**, *8*, No. e1002443.
(11) Dar, R. D.; Weiss, R. Perspective: Engineering noise in biological systems towards predictive stochastic design. *APL Bioeng.* **2018**, *2*, 020901.
(12) Tang, W.; Liu, D. R. Rewritable multi-event analog recording in bacterial and mammalian cells. *Science* **2018**, *360*, No. eaap8992.
(13) Racovita, A.; Prakash, S.; Varela, C.; Walsh, M.; Galizi, R.; Isalan, M.; Jaramillo, A. Engineered gene circuits capable of reinforcement learning allow bacteria to master gameplaying. *bioRxiv*, June 21, 2022. DOI: 10.1101/2022.04.22.489191.
(14) Kumar, S.; Lezia, A.; Hasty, J. Exploiting heterogeneity in coupled, two plasmid systems for dynamic population adaptation. *bioRxiv*, February 19, 2023. DOI: 10.1101/2023.02.19.529072.
(15) Balaban, N. Q.; Merrin, J.; Chait, R.; Kowalik, L.; Leibler, S. Bacterial Persistence as a Phenotypic Switch. *Science* **2004**, *305*, 1622−1625.
(16) Rouches, M. V.; Xu, Y.; Cortes, L. B. G.; Lambert, G. A plasmid system with tunable copy number. *Nat. Commun.* **2022**, *13*, 3908.
(17) Joshi, S. H.-N.; Yong, C.; Gyorgy, A. Inducible plasmid copy number control for synthetic biology in commonly used E. coli strains. *Nat. Commun.* **2022**, *13*, 6691.
(18) Nuñez, I. N.; Matute, T. F.; Del Valle, I. D.; Kan, A.; Choksi, A.; Endy, D.; Haseloff, J.; Rudge, T. J.; Federici, F. Artificial symmetry-breaking for morphogenetic engineering bacterial colonies. *ACS synthetic biology* **2017**, *6*, 256−265.
(19) Bernhardt, T. G.; Roof, W. D.; Young, R. Genetic evidence that the bacteriophage φX174 lysis protein inhibits cell wall synthesis. *Proc. Natl. Acad. Sci. U. S. A.* **2000**, *97*, 4297−4302.
(20) Din, M. O.; Danino, T.; Prindle, A.; Skalak, M.; Selimkhanov, J.; Allen, K.; Julio, E.; Atolia, E.; Tsimring, L. S.; Bhatia, S. N.; Hasty, J. Synchronized cycles of bacterial lysis for in vivo delivery. *Nature* **2016**, *536*, 81−85.
(21) Gupta, S.; Ross, T. D.; Gomez, M. M.; Grant, J. L.; Romero, P. A.; Venturelli, O. S. Investigating the dynamics of microbial consortia in spatially structured environments. *Nat. Commun.* **2020**, *11*, 2418.
(22) Volfson, D.; Cookson, S.; Hasty, J.; Tsimring, L. S. Biomechanical ordering of dense cell populations. *Proc. Natl. Acad. Sci. U.S.A.* **2008**, *105*, 15346−15351.
(23) Rudge, T. J.; Steiner, P. J.; Phillips, A.; Haseloff, J. Computational modeling of synthetic microbial biofilms. *ACS synthetic biology* **2012**, *1*, 345−352.
(24) Jang, S. S.; Oishi, K. T.; Egbert, R. G.; Klavins, E. Specification and simulation of synthetic multicelled behaviors. *ACS synthetic biology* **2012**, *1*, 365−374.
(25) Nagarajan, K.; Ni, C.; Lu, T. Agent-based modeling of microbial communities. *ACS synthetic biology* **2022**, *11*, 3564−3574.
(26) Warren, M. R.; Sun, H.; Yan, Y.; Cremer, J.; Li, B.; Hwa, T. Spatiotemporal establishment of dense bacterial colonies growing on hard agar. *eLife* **2019**, *8*, No. e41093.
(27) Tan, C.; Marguet, P.; You, L. Emergent bistability by a growth-modulating positive feedback circuit. *Nat. Chem. Biol.* **2009**, *5*, 842−848.
(28) Santos-Moreno, J.; Schaerli, Y. Using synthetic biology to engineer spatial patterns. *Adv. Biosys.* **2019**, *3*, 1800280.
(29) Basu, S.; Gerchman, Y.; Collins, C. H.; Arnold, F. H.; Weiss, R. A synthetic multicellular system for programmed pattern formation. *Nature* **2005**, *434*, 1130−1134.
(30) Luo, N.; Wang, S.; You, L. Synthetic pattern formation. *Biochemistry* **2019**, *58*, 1478−1483.
(31) Miano, A.; Liao, M. J.; Hasty, J. Inducible cell-to-cell signaling for tunable dynamics in microbial communities. *Nat. Commun.* **2020**, *11*, 1193.

https://doi.org/10.1021/acssynbio.3c00617
ACS Synth. Biol. XXXX, XXX, XXX−XXX